

Time-dependent fiber bundles with local load sharing. II. General Weibull fibers

S. Leigh Phoenix*

Department of Theoretical and Applied Mechanics, Cornell University, Ithaca, New York 14853, USA

William I. Newman†

Departments of Earth and Space Sciences, Physics and Astronomy, and Mathematics, University of California, Los Angeles, California 90095, USA

(Received 10 July 2009; published 17 December 2009)

Fiber bundle models (FBMs) are useful tools in understanding failure processes in a variety of material systems. While the fibers and load sharing assumptions are easily described, FBM analysis is typically difficult. Monte Carlo methods are also hampered by the severe computational demands of large bundle sizes, which overwhelm just as behavior relevant to real materials starts to emerge. For large size scales, interest continues in idealized FBMs that assume either equal load sharing (ELS) or local load sharing (LLS) among fibers, rules that reflect features of real load redistribution in elastic lattices. The present work focuses on a one-dimensional bundle of N fibers under LLS where life consumption in a fiber follows a power law in its load, with exponent ρ , and integrated over time. This life consumption function is further embodied in a functional form resulting in a Weibull distribution for lifetime under constant fiber stress and with Weibull exponent, β . Thus the failure rate of a fiber depends on its past load history, except for $\beta=1$. We develop asymptotic results validated by Monte Carlo simulation using a computational algorithm developed in our previous work [Phys. Rev. E **63**, 021507 (2001)] that greatly increases the size, N , of treatable bundles (e.g., 10^6 fibers in 10^3 realizations). In particular, our algorithm is $\mathcal{O}(N \ln N)$ in contrast with former algorithms which were $\mathcal{O}(N^2)$ making this investigation possible. Regimes are found for (β, ρ) pairs that yield contrasting behavior for large N . For $\rho > 1$ and large N , brittle weakest volume behavior emerges in terms of characteristic elements (groupings of fibers) derived from critical cluster formation, and the lifetime eventually goes to zero as $N \rightarrow \infty$, unlike ELS, which yields a finite limiting mean. For $1/2 \leq \rho \leq 1$, however, LLS has remarkably similar behavior to ELS (appearing to be virtually identical for $\rho=1$) with an asymptotic Gaussian lifetime distribution and a finite limiting mean for large N . The coefficient of variation follows a power law in increasing N but, except for $\rho=1$, the value of the negative exponent is clearly less than $1/2$ unlike in ELS bundles where the exponent remains $1/2$ for $1/2 < \rho \leq 1$. For sufficiently small values $0 < \rho \leq 1$, a transition occurs, depending on β , whereby LLS bundle lifetimes become dominated by a few long-lived fibers. Thus the bundle lifetime appears to approximately follow an extreme-value distribution for the longest lived of a parallel group of independent elements, which applies exactly to $\rho=0$. The lower the value of β , the higher the transition value of ρ , below which such extreme-value behavior occurs. No evidence was found for limiting Gaussian behavior for $\rho > 1$ but with $0 < \beta(\rho+1) < 1$, as might be conjectured from quasistatic bundle models where $\beta(\rho+1)$ mimics the Weibull exponent for fiber strength.

DOI: [10.1103/PhysRevE.80.066115](https://doi.org/10.1103/PhysRevE.80.066115)

PACS number(s): 62.20.M-, 83.80.Ab, 62.20.Hg, 81.05.Qk

I. INTRODUCTION

Over the past two decades fiber bundle models (FBMs) have received ever increasing attention in the physics community to explain a wide range of phenomena observed in the fracture of materials under stress. While they are natural models for natural and manmade fibrous composites, they have been increasingly used to explain failure processes in multiphase crystalline structures, even when grains are not particularly elongated [1]. FBMs have also been used to study failure in atomic lattices, for instance graphene sheets that are the basic structure of carbon nanotubes [2]. Such models have been used to model electrical failure in resistor networks [3] and dielectrics [4] with discrete structure. Part of their attractiveness for studying materials that ostensibly

might seem better modeled using continuum mechanics approaches, is that stress fields calculated using discrete elastic lattice models show near singular behavior near the tips of elongated clusters of failed elements (fibers), yet also allow for dispersed element failure in the vicinity of these tips that has a strong effect on how such clusters might propagate. In addition models for element failure and load sharing can be unambiguously described and are treatable within analytical [5] or Monte Carlo simulation [6] models.

A wide range of phenomena have been of interest, many motivated by organizing features of percolation theory and behavior of critical points in phase transitions. Many phenomena, however, are unique to FBMs and unpredictably may or may not be amenable to mean-field descriptions depending on a small change in a particular model parameter. Among the many phenomena studied are (i) distributions of avalanche sizes (representing sudden progressions of failed fibers that intermittently terminate [7–9]), (ii) size effects where strength or lifetime may progressively decrease to

*slp6@cornell.edu

†win@ucla.edu

zero or reach a limit as system size increases and the geometry of subcritical failure structures changes radically, (iii) brittle failure with extreme localization [10] versus quasiductile behavior with dispersed element failure, the transition triggered by small changes in certain parameter values, (iv) the scaling of lifetime distributions with load level, just to name a few. Much of the pre-1985 FBM work was reviewed in the forerunner of this paper [6] so we will refer mainly to more recent work as it relates to the above-mentioned phenomena and results in the paper.

The basic fiber bundle model in this paper [local load sharing (LLS) together with the Weibull power-law fiber model] was first studied in its full parametric form by Phoenix and Tierney [11]. The fiber model traces back to Coleman [12]. Newman and Phoenix [6] considered a restricted version of this model where the lifetime of a fiber under fixed load followed an exponential distribution rather than the more general Weibull distribution here.

Using the same exponential lifetime version with the same power-law sensitivity to load level but in some respects a more general load sharing model, a similar FBM was studied by Curtin and Scher [13] and Curtin, Pamel and Scher [14]. These were important works that made some key observations regarding parameter ranges for which dispersed (quasiductile) failure processes would occur versus localized (brittle) failure. They also made important observations in the latter case regarding system size effects and the time scales required to first develop a dominant crack (among many competing cracks), and then for the crack to continue to grow to catastrophic size resulting in terminal failure.

We also mention related work by Herrmann and co-workers [15] who examined how the behavior of a bundle depends upon the range over which each fiber interacts with its neighbors and for this purpose they used a power-law load redistribution varying as the distance of separation raised to a negative power. Thus low values of the exponent gave approximately equal load sharing and high values approximately local load sharing. Both time dependent bundles with a power law relating fiber time to failure to its load level (with exponentially distributed lifetime under fixed fiber load) as well as Weibull fiber strength in a quasistatic bundle model were studied. They found that both the lifetime version and the strength version exhibited a crossover from mean-field (ductile) to short-range (brittle) behavior and that the point of transition depends on the system's disorder in terms of exponents for strength or lifetime. Also the growth dynamics of the largest crack were radically different in the two limiting regimes of load transfer (limiting exponent values) especially during the first stages of breaking. High values of the strength or lifetime exponent coupled with high values of the stress-redistribution exponent promoted very brittle behavior and the opposite promoted ductile behavior with distributed damage and no localization.

The fiber element failure model of the present paper is based on a thermally activated mechanism involving power-law sensitivity of fiber element lifetime to stress level. The exponent of the power law is proportional to activation energy divided by absolute temperature, as shown by Phoenix and Tierney [11]. However, Ciliberto, and co-workers [16] have considered other versions in two-dimensional spring

networks with quenched disorder. The rupture of a spring element is assumed thermally activated and its lifetime follows an Arrhenius law where its energy barrier is reduced by the local disorder effect on the stress in the element. In effect an effective system temperature arises amplified by the spatial disorder (heterogeneity) of the fiber bundle. In a related work, Yoshioka *et al.* [17] perform calculations showing that the presence of such local stress inhomogeneities results in cracking with an anomalous size effect where the average lifetime decreases as a power of the system size with the exponent depending on external load divided temperature to the power $3/2$ in a modified Arrhenius form.

Recently Toussaint and Hansen [18] considered issues of localization of damage in a tubular quasistatic fuse model, working with a mean-field approach. Depending on the quenched disorder distribution of fuse thresholds (with both power-law lower and upper tails with different exponents) they showed analytically that the system can (i) either stay in a percolation regime up to breakdown, or (ii) beginning at some imposed current, to localize starting from the smallest scale lattice spacing, or (iii) enter a diffuse localization regime where damage starts to concentrate in bands having width scaling as the width of the system, but otherwise being diffuse at smaller scales. Depending on the nature of the quenched disorder on fuse thresholds, a phase diagram of the system was obtained separating these regimes and the current levels for the onset of these possible localizations. Similar to what we will find in the current work, as the system size increases, the once critical values for the exponent of the power-law lower tail of the disorder distribution become unity above which the system completely localizes. Below this value (and for larger systems sizes) a second critical value occurs for this power-law lower tail above which (and below unity) diffuse localization occurs and below which fully diffuse percolation like failure occurs. However this second critical value appears to decrease roughly in inverse proportion to the logarithm of the system size.

In related work, Pradan and Hansen [19] investigated the effects on bundle strength of a lower cutoff in the fiber strength distribution (with an upper cutoff as well, so all fiber strengths were between the lower and upper cutoffs) under both equal load sharing and local load sharing. Under both forms, raising lower strength cut-off level beyond a critical strength value resulted in instant bundle collapse when the weakest fiber failed irrespective of the upper cutoff. Under local load sharing, however, this critical strength value was lower than under equal load sharing and with increasing system size the bundle strength and avalanche statistics were strongly influenced by the chosen value of the lower cutoff, with the bundle eventually becoming no stronger than the lower cutoff. While the fiber strength distributions were time independent, the results again showed that the extreme tails of the distributions control the behavior of very large bundles irrespective of the mean and coefficient of variation (i.e., the standard deviation divided by the mean) of fiber strength. This cutoff effect was also studied by Raischel, Kun, and Herrmann [20] and by Pradhan, Bhattacharyya, and Chakrabarti [21] with similar observations.

Numerical simulations of lattice models of fracture have been used [22] to study the crossover between the regime

controlled by disordered failure (quasiductile) and the regime where localization and crack-like stress concentrations emerge, reflected primarily by continuum fracture mechanics concepts. Nonetheless, scaling laws emerge involving a fracture process zone, whose scaling properties are revealed only upon sampling over many configurations of the disorder. These authors [23] have also contributed a broad review that ties together various models for the size effect phenomenon in the failure of materials. These models span extreme-value statistics, fracture mechanics (including finite boundary effects), R -curve behavior resulting from fracture process zones and fractal effects and fiber bundle models under global and local load sharing, including closely related scalar random fuse models. Also discussed are geometric size effects from the roughness of crack surfaces (self-affine and with other exponents).

In a similar vein, Roux [24] pursued the effects, in equal load sharing bundles, of having narrow quenched disorder and a Gaussian distribution of thermal noise driving the fracture stress of the fibers, and also found the failure to be controlled by an effective temperature translated with respect to the actual one. In related work Roux and Hild [25] studied the influence of growing distributed fiber failures with increasing time or load on the effective interaction Green's function (decaying as the distance raised to a negative power) between broken fiber clusters and nearby surviving fibers in an elastic lattice model. This Green's function was found to become more and more long ranged as the tangent modulus vanished and the reloaded region became narrower and narrower so that the damage development diverged from local load sharing behavior to become closer and closer to the so-called global (or equal) load sharing rule. This was argued to justify use of a mean-field approach as the peak stress is approached.

Looking in more detail at subcritical cluster or crack growth in a load sharing setting treated using fracture mechanics ideas but with probabilities for step-by-step growth or arrest mimicking a fiber bundle setting, Hilde and Roux [26] calculated the probability a crack will start at one size and reach some larger size, eventually taking a limit as this size became infinite. In the model the rate of crack growth was governed by a power-law exponent playing much the role of the exponent of the present work governing sensitivity of fiber lifetime to load level. In essence they found that, as the exponent was increased, the time taken to grow from some size to catastrophic size became increasingly dominated by the first few time steps.

Recent contributions by Bazant and co-workers [27] have provided an insightful context for the roles of fiber bundle models in capturing the two disparate types of failure, ductile versus brittle, in a broad range of materials of engineering importance. They also elucidated the interplay of the critical size scales over which both types of failure activity can occur in the same material and how this interplay affects the extent to which the classical Weibull distribution (whether in its three parameter or two parameter form) can accurately describe the strength behavior of a given material system over structural size scales and failure probability levels spanning many orders of magnitude. This issue is crucial in justifying the extrapolation of strength test results on relatively few

laboratory scale samples to much larger structures that have requirements for extremely low probabilities of failure. This same issue is important in the current work, which assumes Weibull behavior at the fiber element level but can yield dramatically non-Weibull behavior at the large bundle level depending on the parameter values.

Related work with major technological implications on development of materials is that of Pugno [2], who shows that contrary to widely held notions, ropes and cables constructed from hierarchical arrangements of bundles of carbon nanotubes are unlikely to achieve more than a very small fraction of the flaw-free strength of a graphene sheet, all because of the emergence and interaction of defects and bond failures, whether as imperfections occurring during growth or the result of thermal activation coupled with the applied stress.

Observations in all the above works relate in one way or another to the results in this paper. We will restrict ourselves to one-dimensional bundles under local load sharing but with power-law dependence of lifetime to load level in a Weibull lifetime framework. We systematically investigate mainly the behavior of lifetime distributions for a broad variety of parameter ranges for the power-law and Weibull exponents.

Organization of the paper

The remainder of the paper is organized as follows. Section II gives an overview of the fiber failure model, the load sharing rules and the parameter cases considered together with bundle sizes and replications in the Monte Carlo simulations. Section III considers ductile-like bundle behavior beginning with cases involving very small values of ρ and working upward. Section III A mainly discusses observations from the Monte Carlo simulations, including maps of how the mean and coefficient of variation in bundle lifetime depend on values of the parameters ρ and β and bundle size N . Section III B gives a theoretical perspective on behavior observed and how it relates to known results on equal load sharing bundles under the same fiber lifetime model.

Section IV then considers various cases of $\rho > 1$ where brittle-like bundle behavior occurs with weakest-link character in terms of a characteristic distribution function for failure of a link. Section IV A discusses the Monte Carlo results and scalings that organize the data for increasing bundle size, and Sec. IV B derives asymptotic results that accurately capture the weakest-link behavior seen in terms of time to formation of a critical cluster, and time for it to traverse the bundle as a catastrophic crack. Section V concludes with a summary of the main results.

II. DESCRIPTION OF THE MODEL FOR FIBER LIFETIME AND LOCAL LOAD SHARING IN THE BUNDLE

A. Load sharing models

In our previous paper [6], we considered the behavior of the lifetime distribution of a one-dimensional (1D) bundle of N fibers under an applied load $L > 0$ per fiber, and assumed two different laws for fiber load sharing, once fibers began to

fail. The first law was called equal load sharing (ELS) wherein the load on a fiber at its time of failure was redistributed in equal portions onto all of its surviving neighbors so that the load concentration on each fiber was

$$K_j = \frac{N}{N-j}, j = 1, 2, 3, \dots, \quad (1)$$

where N is the number of fibers in the bundle and j is the number that have failed. The second law was LLS wherein the load on a fiber at its time of failure was redistributed equally onto its two closest surviving neighbors, one on each side. That is, the load concentration factor under LLS is

$$K_r = \frac{2+r}{2}, \quad r = 1, 2, 3, \dots, \quad (2)$$

where r is the number of contiguous failed neighbors, counting on both sides.

B. Fiber lifetime model

In the current study, we consider the behavior of bundles where individual fibers follow a more general Weibull form for their lifetime distribution and now have memory of their past load history. Specifically, we assume that when under a given, non-negative load history, $\ell(t), t \geq 0$, individual fibers have independent and identically distributed lifetimes that have distribution function

$$F[t; \ell(\cdot)] = 1 - \exp \left\{ - \left\{ \frac{1}{t_{\text{ref}}} \int_0^t \left[\frac{\ell(s)}{\ell_{\text{ref}}} \right]^\rho ds \right\}^\beta \right\}, \quad t \geq 0, \quad (3)$$

where t_{ref} and ℓ_{ref} are a reference time and reference load, respectively. Thus, under a constant load, individual fibers now follow a Weibull distribution for lifetime with shape parameter $\beta > 0$. Of course, once fibers begin to fail as members of a bundle, the loads on their survivors will no longer all be identical in time and their load histories must be accounted for as failure progresses. Our previous work [6], under $\beta=1$, is a special case of this framework whereby the memoryless property holds, and the treatment of different fiber load histories is greatly simplified.

C. Motivating observations from our previous study [6]

In our previous work under LLS and $\beta=1$, the statistics for the lifetime of a bundle proved highly dependent on the value of ρ where $0 < \rho \leq 1$ gave very different lifetime behavior from $\rho > 1$, not only in the form of the lifetime distribution but also in the scaling of the mean and standard deviation for lifetime with bundle size, N . For $\rho > 1$, bundles showed brittle-like behavior and, although many small clusters of contiguous fiber breaks formed and began to grow depending on the value of $\rho-1$, eventually one cluster would become dominant and catastrophic, with a growth rate influenced little by small clusters consumed in its path. Such bundles also showed decreasing lifetime and other subtle cluster growth characteristics with increasing bundle size, N . When $\rho=1$, the lifetime distribution was found to be asymptotically Gaussian, as N increased, and had a size-independent mean lifetime and a standard deviation of lifetime decreasing as $N^{-1/2}$. For $0 < \rho < 1$, i.e., ρ only slightly smaller than unity, Gaussian behavior occurred as well, though with mean lifetime actually increasing slowly with N and the standard deviation decreasing more slowly than $N^{-1/2}$. However, when $0 < \rho \ll 1$, i.e., in the extreme where ρ is close to zero, Gaussian lifetime behavior gave way to a double-exponential lifetime distribution, which is one of the limiting distributions in the statistical theory of extremes for the maximum of an independent and identically distributed random variable sequence.

Generally in the regime $0 < \rho \ll 1$, increasing numbers of break clusters would form and grow as time increased, but these would tend to grow slowly and in sum would consume fewer neighboring fibers around them (all overloaded) than would fail at random locations elsewhere due to the applied load alone, i.e., without any load enhancement from failed neighbors. Thus, failure resulted from a progressive consumption process of the bundle with the eventual linking of the many clusters in a “ductile”-like manner, rather than by the emergence of a dominant crack as occurred for $\rho > 1$.

A key feature driving these observed behavioral differences with the value of ρ was that, when a fiber failed and its load was redistributed between its two flanking survivors, the magnitude of ρ determined whether the sum of failure rates for all surviving fibers would decrease ($\rho < 1$), increase ($\rho > 1$), or remain the same ($\rho = 1$) compared to this failure rate sum before the fiber failed. Since surviving fibers had no memory of past load history (i.e., $\beta=1$ in the fiber model described shortly), their remaining lifetimes at a given point in time were dependent on the current configuration of failed and surviving fibers, but not on the past fiber failure times, so not on their previous load histories. Furthermore, for $\rho=1$, the sum of the failure rates for all surviving fibers was the same, irrespective of how many fibers had failed up to that time, and the actual pattern of surviving fibers and associated load redistribution. Thus the case $\rho=1$ could be solved exactly, irrespective of the load sharing rule provided that the overall load was conserved.

Although the statistics of times between fiber failures become much more complex when $\beta \neq 1$, it is still reasonable to investigate, as we do in this paper, the extent to which the previously mentioned behavioral characteristics seen for $\beta=1$ also arise for the cases $\beta < 1$ and $\beta > 1$. Again, we will find that the overall failure process can be separated into two regimes: A ductile-like regime for $0 < \rho \leq 1$ and a brittle-like regime for $1 < \rho$. We will investigate these regimes through Monte Carlo simulation coupled with asymptotic analysis where possible. For each parameter pair (ρ, β) , we consider bundle sizes 8, 16, 32, 64, 128, 256, ..., 1 048 576 with 1024 replications for each case. Note that these large bundle size calculations are possible since our algorithm, developed in Newman and Phoenix [6] is $\mathcal{O}(N \ln N)$ in contrast with former algorithms which were $\mathcal{O}(N^2)$. Without loss of generality, we shall take $t_{\text{ref}} = \ell_{\text{ref}} = 1$ in all Monte Carlo simulations and assume the load on the bundle is $\ell(t) = L > 0$ where we take $L=1$.

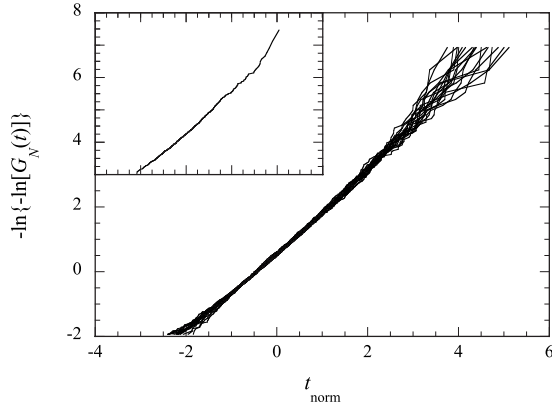


FIG. 1. Distribution scaling for $\rho=0.1$, $\beta=1$ adapted from Newman and Phoenix (2001), where a straight line limit occurs with slope ≈ 1.27 and intercept ≈ -0.45 . The inset shows the line shape for the largest bundle size $N=1\ 048\ 576$.

III. DUCTILE-LIKE BEHAVIOR FOR $0 < \rho \leq 1$

A. Monte Carlo results

We consider first the case of small $0 < \rho \ll 1$ and $\beta=0.5$, 1.0, and 2.0. Motivated by our previous observations [6] shown in Fig. 1 for $\rho=0.1$ and $\beta=1$, we have plotted the corresponding Monte Carlo simulation results for $\beta=0.5$ and $\beta=2.0$ in Figs. 2 and 3, respectively. Note that in all three figures the parameter product $\beta\rho$ satisfies $0 < \beta\rho \ll 1$.

For this small ρ case, Newman and Phoenix [6] noted that, early in the bundle collapse process, the shedding of load from a failed fiber to its two flanking survivors would result in very little increase in failure rates of the two accepting it. In fact, in summing the failure rates for all the survivors after a fiber failure event, the time until the next fiber failed (which was exponentially distributed since $\beta=1$) would tend to be longer than before since there was now one less fiber and the vast majority were all carrying their original loads. Thus, despite the localized load redistribution, as time went on there was virtually no tendency to develop a large isolated cluster that might grow unstable, since for any cluster, the sum of the failure rates on the many nearby non-

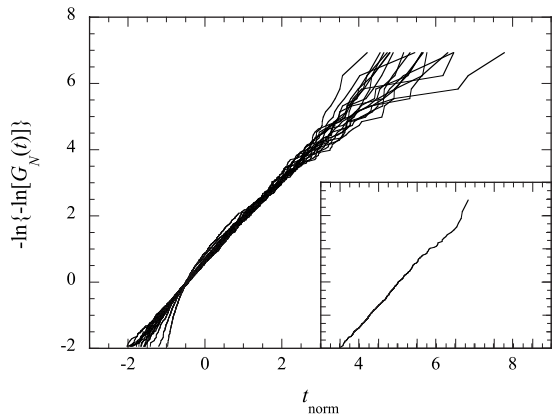


FIG. 2. Distribution scaling for $\rho=0.1$, $\beta=0.5$ where a straight line limit occurs with slope ≈ 1.27 and intercept ≈ -0.45 . The inset shows the line shape for the largest bundle size $N=1\ 048\ 576$.

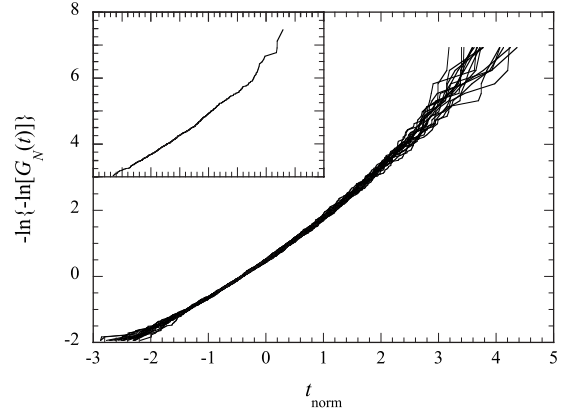


FIG. 3. Distribution scaling for $\rho=0.1$, $\beta=2$, where a straight line limit fails to occur on this scaling. The inset shows the line shape for the largest bundle size $N=1\ 048\ 576$.

overloaded fibers would overwhelm the sum of the rates for the two flanking survivors to the cluster. Consequently the failure process would strongly favor nucleation of clusters rather than extension of existing ones. In some respects a large failure cluster of k failed fibers would act effectively to block the failure process as the failure rate of its two flanking survivors would be far less than the sum of the failure rates of $k+2$ surviving fibers not next to failed fibers.

Thus, for $0 < \rho \ll 1$, and other β values, one might speculate that the system behaves as the longest lived of N asymptotically independent “elements,” consisting perhaps of small collections of fibers in some failure resistant, load sharing state rather than individual fibers, since ultimately the loads must increase greatly on the fibers in these collections of survivors. In other words, there exists some “strongest characteristic link” distribution function for failure, denoted $Q(t)$, with survival function $\Omega(t)=1-Q(t)$ such that the distribution function for bundle failure, $G_N(t)$, behaves as

$$\begin{aligned}
 G_N(t) &= [Q(t)]^N = [1 - \Omega(t)]^N \\
 &\approx \exp[-N\Omega(t)] \\
 &\approx \exp\left\{-\exp\left[-\ln\left(\frac{1}{N\Omega(t)}\right)\right]\right\}, \quad (4)
 \end{aligned}$$

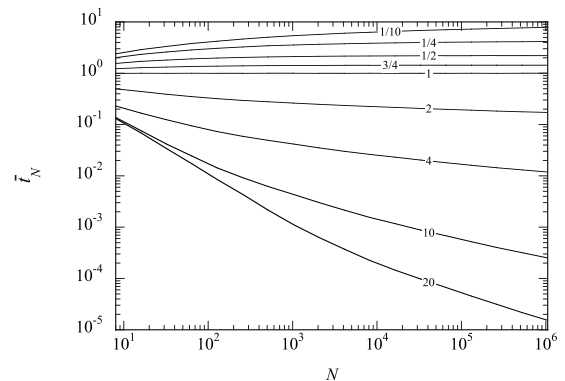


FIG. 4. Bundle mean lifetime \bar{t}_N as $N \rightarrow \infty$ for $0.1 \leq \rho \leq 20$ and $\beta=1$.

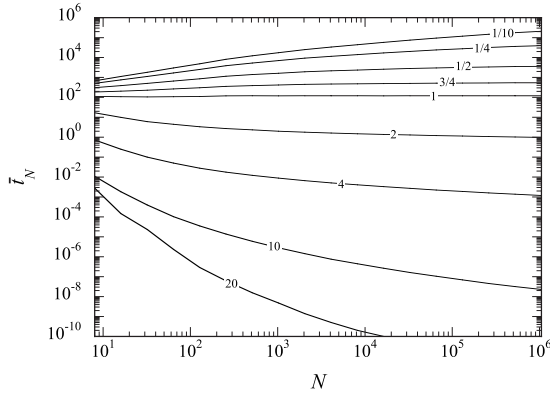


FIG. 5. Bundle mean lifetime \bar{t}_N as $N \rightarrow \infty$ for $0.1 \leq \rho \leq 20$ and $\beta=0.2$.

for large N . Newman and Phoenix [6] observed through Monte Carlo simulations that

$$G_N(t) \approx \exp \left\{ - \exp \left[- a \left(\frac{t - \bar{t}_N}{\bar{\sigma}_N} \right) + b \right] \right\}, \quad (5)$$

with $a \approx 1.27$ and $b \approx -0.45$ for N large as seen in Fig. 1 where straight line behavior emerges as $N \rightarrow \infty$.

This observation motivates us to consider whether similar behavior occurs for other values of β , whereby

$$\ln \left(\frac{1}{N \Omega_\beta(t)} \right) \approx a \left(\frac{t - \bar{t}_{N,\beta}}{\bar{\sigma}_{N,\beta}} + b \right), \quad (6)$$

for N large or

$$N \Omega_\beta(t) \approx \exp \left\{ - a \left(\frac{t - \bar{t}_{N,\beta}}{\bar{\sigma}_{N,\beta}} + b \right) \right\}, \quad (7)$$

for N large. Indeed for the case $\rho=0.1$ and $\beta=0.5$, as shown in Fig. 2, the same straightline scaling limit occurs for the shape of the lifetime distribution as $N \rightarrow \infty$, again with $a \approx 1.27$ and $b \approx -0.45$, though for small bundle sizes N , the distribution shapes are initially opposite in curvature to those in Fig. 1. This limiting, straight line scaling behavior, however, does not universally occur for higher $\beta > 1$ values, as Fig. 3 shows for the case $\beta=2$, $\rho=0.1$, where curvature de-

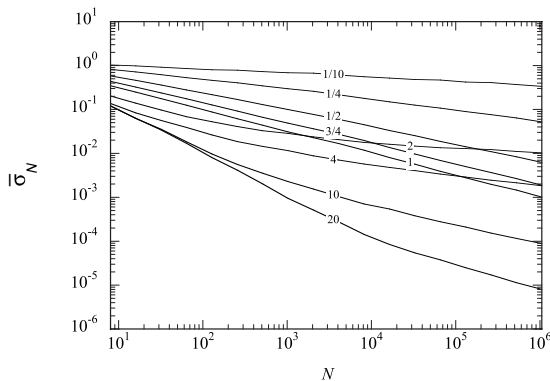


FIG. 6. Standard deviation of bundle lifetime $\bar{\sigma}_N$ as $N \rightarrow \infty$ for $0.1 \leq \rho \leq 20$ and $\beta=1$.

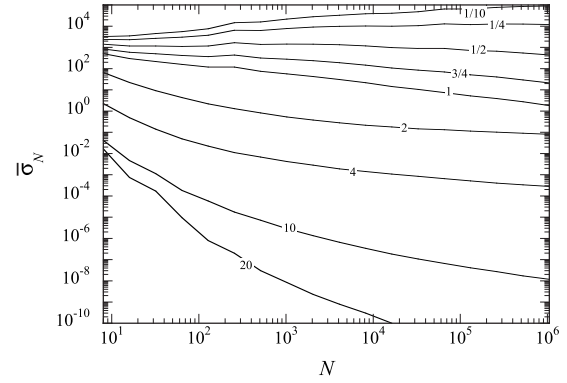


FIG. 7. Standard deviation of bundle lifetime $\bar{\sigma}_N$ as $N \rightarrow \infty$ for $0.1 \leq \rho \leq 20$ and $\beta=0.2$.

velops in the shape of the limiting lifetime distribution.

To further investigate the size scaling of lifetime for small ρ , we study the behavior of the mean \bar{t}_N and standard deviation $\bar{\sigma}_N$ as $N \rightarrow \infty$ and for various ρ values from very small to large. Figures 4 and 5 allow a comparison of results for \bar{t}_N for the cases $\beta=1$ and $\beta=0.2$, respectively. For the smallest ρ values, the mean lifetime increases in N and is similar in shape for the two cases of β , although the growth is much more rapid in N for the smaller value $\beta=0.2$. The plot is clearly not linear on log-log coordinates, thus appearing to rule out a simple power law and while one cannot rule out a fixed limit for $0 \ll \rho < 1$ such a limit would appear to be much larger for small β . Thus for smaller bundles with very small ρ , the tendency for increasing mean lifetime with increasing bundle size N reflects the general tendency for a redundant, nonload sharing system of N parallel elements to have increasing lifetime, since load redistribution is ineffective in the former and nonexistent in the latter. In essence, N has to be very large for $1 \ll N^\rho$ whereby load redistribution can exert a major limiting effect on lifetime.

Figures 6 and 7 show the corresponding behavior for the lifetime standard deviation $\bar{\sigma}_N$. For $\beta=1$ and $0 < \rho \leq 1$, $\bar{\sigma}_N$ appears to decrease with N , following the scaling $1/N^q$ for some $0 < q \leq 1/2$, and for $\rho=1$ we know that $q=1/2$ [6]. The same, however, is not true when $\beta=0.2$, as shown in Fig. 7, where $\bar{\sigma}_N$ increases with N for $0 < \rho < 1/2$.

On the other hand, the coefficient of variation (CV),

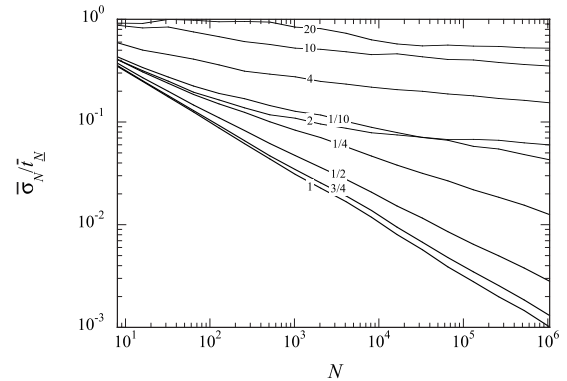


FIG. 8. CV of bundle lifetime $\bar{\sigma}_N/\bar{t}_N$ as $N \rightarrow \infty$ for $0.1 \leq \rho \leq 20$ and $\beta=1.0$.

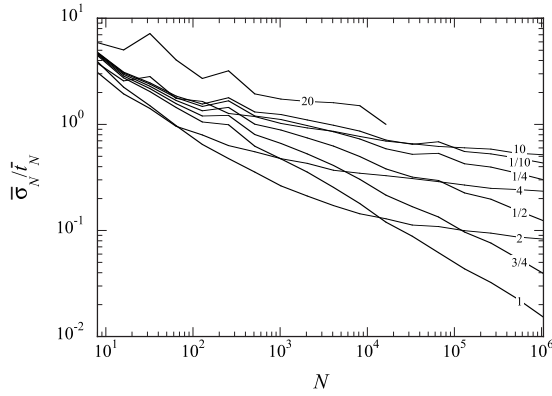


FIG. 9. CV of bundle lifetime $\bar{\sigma}_N/\bar{t}_N$ as $N \rightarrow \infty$ for $0.1 \leq \rho \leq 20$ and $\beta=0.2$.

namely, $\bar{\sigma}_N/\bar{t}_N$, behaves differently from \bar{t}_N and $\bar{\sigma}_N$, and, as shown in Figs. 8–10, decreases as N increases irrespective of the values of ρ . The straight line log-log plots indicate that there is a strong tendency for power-law behavior when $0 < \rho \leq 1$, although for very small β the bundle sizes and resolution to fully confirm this would need to be much larger than permitted by our current computational capability. Nonetheless, there are several important trends.

The most striking feature in Figs. 8–10 is that the rate of decrease in relative variability with increasing bundle size N is largest when $\rho=1$ irrespective of β and follows a power-law scaling $1/N^q$ as $N \rightarrow \infty$ with exponent $q=1/2$. In the case of $\beta=1$ and $\rho=1$ (Fig. 8), we know [6] that the overall rate of failure of fibers is independent of the actual choice of load sharing rule and in fact is constant, provided that the loads on individual fibers sum to the applied bundle load L . However, for $\beta=0.2$ and $\rho=1$ (Fig. 9), the dependence of fiber failure rates on past fiber load histories rules out making such a blanket statement, yet this value still provides the most rapid decrease in relative variability, which again appears to asymptotically follow a power law with slope $q=1/2$.

Next we consider the case $1/2 \leq \rho \leq 1$ and focus first on $\rho=1/2$. Guided by our observations in Newman and Phoenix [6] for $\rho=1/2$ and $\beta=1$, we plot in Fig. 11 Monte Carlo simulation results for $\rho=1/2$ and $\beta=2.0$ using Gaussian co-

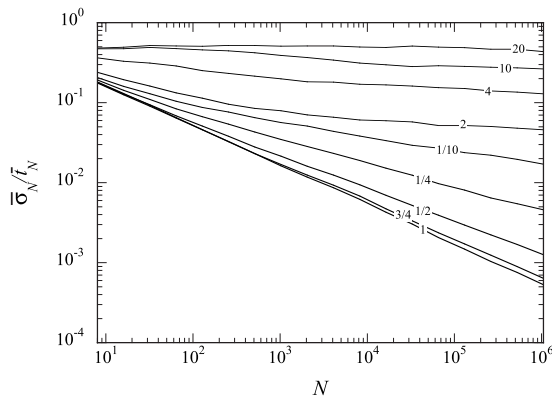


FIG. 10. CV of bundle lifetime $\bar{\sigma}_N/\bar{t}_N$ as $N \rightarrow \infty$ for $0.1 \leq \rho \leq 20$ and $\beta=2.0$.

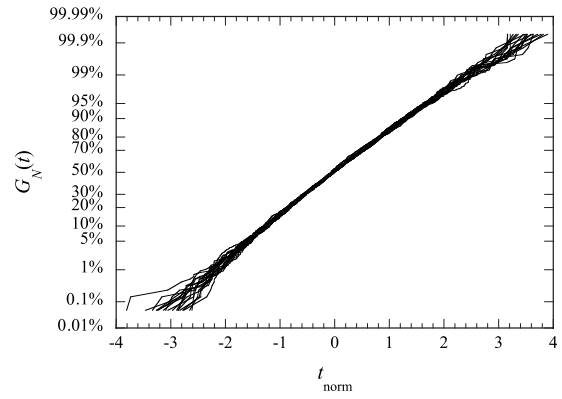


FIG. 11. Distribution scaling using Gaussian coordinates for $\rho=0.5$, $\beta=2$ and increasing N , showing linear limiting behavior as $N \rightarrow \infty$.

ordinates whereby a true Gaussian distribution would plot as a straight line. The normalized time to failure $t_{\text{norm}} \equiv (t - \bar{t}_N)/\bar{\sigma}_N$ converges to a straight line even more rapidly than for $\beta=1$ in Newman and Phoenix [6], suggesting even stronger asymptotic Gaussian behavior. However, the CV asymptotically has exponent $q=0.425$ in $1/N^q$ and, nevertheless, is only slightly larger than the observed value of about 0.41 for $\beta=1$.

For the case $\rho=0.75$ and $\beta=1$, Newman and Phoenix [6] found asymptotic Gaussian behavior for the normalized time to failure, t_{norm} with a standard deviation scaling as $1/N^q$ where $q=0.4709$. Although not shown, the case $\beta=2$ and $\rho=0.75$ has even more rapid convergence to an asymptotic Gaussian distribution with $q=0.485$. We also considered the asymptotic behavior of the lifetime distribution for the much smaller value, $\beta=0.2$, again with $\rho=0.75$. When normalized according to $t_{\text{norm}} \equiv (t - \bar{t}_N)/\bar{\sigma}_N$ the distributions plotted on Gaussian coordinates are extremely curved though with some tendency to straighten as $N \rightarrow \infty$. Plotting the results as though the bundle lifetime follows a log-Gaussian or lognormal distribution [i.e., $\ln(t)$ follows a Gaussian distribution] was much more illuminating. Figure 12 shows plots of the normalized log-lifetimes according to $\ln(t)_{\text{norm}} \equiv [\ln(t) - \ln(\bar{t}_N)]/\sigma[\ln(t)]_N$ for $N=2^3, 2^{15}, 2^{16}, 2^{18}$, and 2^{20} . We ob-

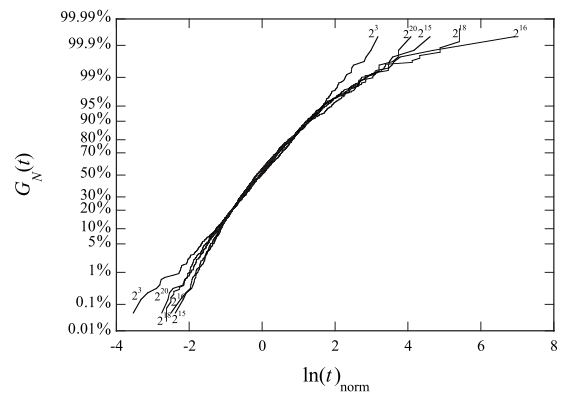


FIG. 12. Distribution scaling using log-Gaussian coordinates for $\rho=0.5$, $\beta=0.2$ and increasing N , suggesting eventual linear limiting behavior as $N \rightarrow \infty$.

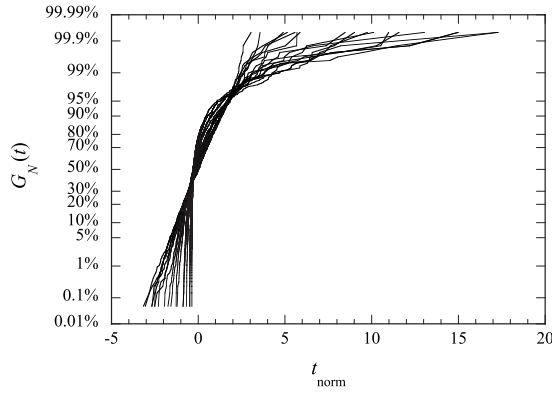


FIG. 13. Distribution scaling for $\rho=1$ and $\beta=0.2$ using Gaussian coordinates where a straight line limit eventually occurs as $N \rightarrow \infty$.

serve that whereas the normalized log lifetimes of the smallest bundles have near straight line behavior on lognormal coordinates, the curvature progressively increases for bundle sizes up to about $N=2^{15}=32\,768$, but thereafter the curvature decreases so that the lines become fairly straight over most of the probability range by $N=2^{20}=1\,048\,576$. In practical terms, the lifetime of large (and small) bundles is log normal. However, it should be noted that since the coefficient of variation decreases in N , asymptotic lognormal behavior implies asymptotic normal behavior (through a Taylor series expansion) albeit with extremely slow convergence when β is small. Finally we note that similar behavior but with slower convergence was seen also for $\beta=0.1$ and $\rho=0.75$.

For the case $\rho=1$, Figs. 13–15 show plots of $t_{\text{norm}} \equiv (t - \bar{t}_N) / \bar{\sigma}_N$ for the cases $\beta=0.2, 0.5$, and 2.0 , respectively, where the case $\beta=1$ was given in [6]. In all cases, a Gaussian limit occurs as $N \rightarrow \infty$, although the convergence is rather slow in the case of $\beta=0.2$. Thus, the behavior is similar to that for $\beta=1$. Numerical results were obtained for $\beta=0.1$ and $\rho=1$, but convergence to a Gaussian form, although likely, would require N to be 100 times larger and would be more rapid on lognormal coordinates. Overall we see asymptotic Gaussian behavior emerging in the region $1/2 \leq \rho \leq 1$.

Figure 16 summarizes the power-law exponents q for the $1/N^q$ behavior (slopes) seen in Figs. 8–10, and from addi-

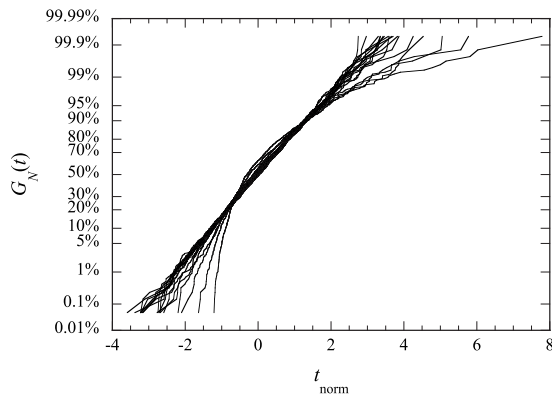


FIG. 14. Distribution scaling for $\rho=1$ and $\beta=0.5$ using Gaussian coordinates where a straight line limit eventually occurs as $N \rightarrow \infty$.

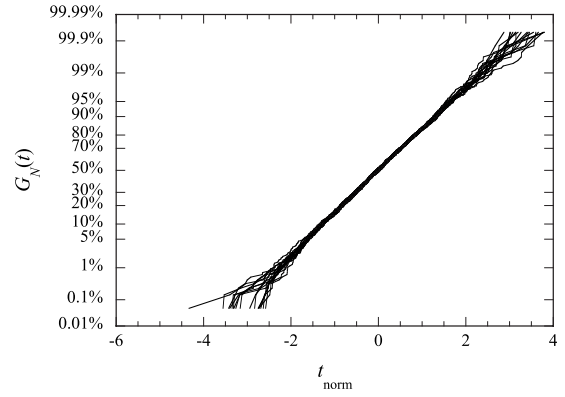


FIG. 15. Distribution scaling for $\rho=1$ and $\beta=2.0$ using Gaussian coordinates where a straight line limit eventually occurs as $N \rightarrow \infty$.

tional calculations for $\beta=0.1$ for various values $0 \leq \rho \leq 1$. Clearly, as β becomes smaller, the exponents are driven to lower values, until even for $\rho=1$ the exponent appears to fall short of $q=1/2$ for $\beta=0.1$. Caution must be exercised, however, since the results for $\beta=0.1$ have more noise and the limiting slope was not quite reached for $N=10^6$ and would require $N=10^8$ fibers. Although the final slope observed was $q \approx -0.45$, there is no reason to believe that it would not eventually become $1/2$ as $N \rightarrow \infty$.

B. Further theoretical considerations

At the other extreme in Fig. 16, the points corresponding to $\rho=0$ were obtained by treating the bundle as if load redistribution does not occur, and thus has no effect on the failure rate since the load on a surviving fiber acts as though it is always 1. Then the distribution function for fiber lifetime is simply

$$Q(t) = 1 - \exp(-t^\beta), \tag{8}$$

and thus

$$G_N(t) = [Q(t)]^N = \{1 - \exp(-t^\beta)\}^N \approx \exp\{-N \exp(-t^\beta)\}, \tag{9}$$

for N large, or

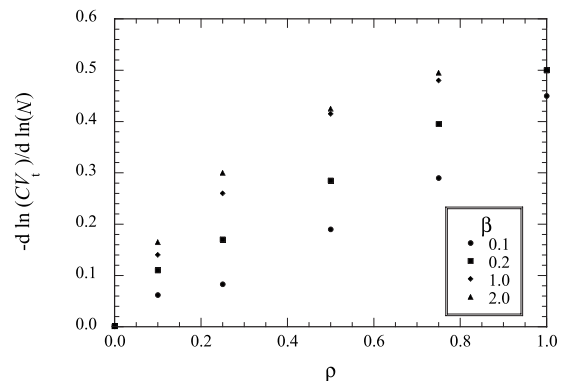


FIG. 16. Scaling of exponents q as in Figs. 8–10 versus ρ for $\beta=0.1, 0.2, 1.0$, and 2.0 .

$$G_N(t) \approx \exp\{-\exp[-(t^\beta - \ln N)]\}. \quad (10)$$

For $\beta=1$, this has the form of the Gumbel distribution with location parameter $\ln N$ and scale parameter unity, and the mean, standard deviation, and coefficient of variation in this distribution function are well known to be, respectively,

$$t_N \approx \ln N + \gamma, \quad (11)$$

$$\sigma_N \approx \frac{\pi}{\sqrt{6}}, \quad (12)$$

and

$$CV_N \approx \frac{\pi}{\sqrt{6}(\ln N + \gamma)}, \quad (13)$$

where $\gamma \approx 0.57722$ is the Euler-Mascheroni constant. For smaller $0 < \beta < 1$ and $1/\beta$ an integer, a Taylor Series expansion in t about $(\ln N)^{1/\beta}$ yields the approximation $t^\beta - \ln N \approx \beta(\ln N)^{(\beta-1)/\beta} \{t - (\ln N)^{1/\beta}\}$ with relative error $O([t - (\ln N)^{1/\beta}]/[(\ln N)^{1/\beta}])$. Again this yields, approximately, the well known two-parameter Gumbel distribution so that

$$t_{N,\beta} \approx (\ln N)^{1/\beta} \left[1 + \frac{\gamma}{\beta \ln N} \right], \quad (14)$$

$$\sigma_{N,\beta} \approx \frac{\pi}{\beta\sqrt{6}} [\ln N]^{(1-\beta)/\beta}, \quad (15)$$

and

$$CV_{N,\beta} = \frac{\pi}{\beta\sqrt{6}(\ln N + \gamma/\beta)}. \quad (16)$$

The log-log slope is thus

$$\frac{d \ln(CV_{N,\beta})}{d \ln(N)} \approx -\frac{1}{\ln N}, \quad (17)$$

and so goes to zero as $N \rightarrow \infty$ as we have plotted in Fig. 16 for $\rho=0$. The trends in Fig. 16 are certainly consistent with this result, including slowed convergence as $N \rightarrow \infty$ for smaller β . Thus for the case $\beta=1$ and $\rho=0$ we can write

$$G_N(t) \approx \exp\left\{-\exp\left[-\frac{\pi}{\sqrt{6}}\left(\frac{t - (\ln N + \gamma)}{\pi/\sqrt{6}} + \frac{\gamma}{\pi/\sqrt{6}}\right)\right]\right\}, \quad (18)$$

or

$$G_N(t) \approx \exp\left\{-\exp\left[-\frac{\pi}{\sqrt{6}}\left(t_{\text{norm}} + \frac{\gamma}{\pi/\sqrt{6}}\right)\right]\right\}, \quad (19)$$

where

$$t_{\text{norm}} = \frac{t - (\ln N + \gamma)}{\pi/\sqrt{6}}. \quad (20)$$

Evaluating the constants in G_N , we find that $\pi/\sqrt{6}=1.283$ and $\gamma/(\pi/\sqrt{6})=0.4499$. (Note that the asymptotic analysis performed for $0 < \beta < 1$ results in the same behavior.) Remarkably, these values are very close to the values $a=1.27$

and $-b=0.45$ for the linear behavior seen in Figs. 1 and 2, though this observation offers no insight into the apparent absence of such behavior in Fig. 3 for $\beta=2$. We note, however, that when $\beta=2$ the standard deviation (15) can be seen to follow $\sigma_{N,2} \approx 1/(2\sqrt{\ln N})$ and so decreases in N rather than increasing. Such decreasing behavior occurs, in fact, for all $\beta > 1$ so $\beta=1$ is a transition point that may subtly affect the local scaling.

Another issue is the rate of failure of fibers and the fraction typically surviving at a time equal to the mean time to bundle failure, namely $t=t_N$. The fraction surviving on average is

$$\frac{N_s}{N} = 1 - F(t) \approx \exp(-t_N^\beta) \approx \frac{1}{N} \left[1 + \frac{\gamma}{\beta \ln N} \right]^\beta, \quad (21)$$

so that for bundles that achieve the mean lifetime there will only be a few fibers left irrespective of how many there were at the start and irrespective of β . In fact, the value of β has its major effect at short times. When β is large, some time must pass before fibers begin to fail, whereas when β is small, there is a burst of fiber breaks early in the life of the bundle that rapidly depletes the number of fibers, but thereafter the failure rate slows down sufficiently to compensate for the early depletion, as can be seen in comparing plots in Figs. 4 and 5 for given ρ values. Nonetheless we expect a major difference in lifetime behavior between ρ small, say $\rho=0.1$, versus the limiting case $\rho=0$, since even when few fibers remain and N is large, the loads must eventually become very large on the few survivors when $\rho=0.1$ to dramatically affect the terminal failure rate. For instance, the failure rates of the survivors will eventually be accelerated by the factor

$$\frac{N}{N_s} = \left\{ \frac{N}{[1 + \gamma/(\beta \ln N)]^\beta} \right\}^\rho, \quad (22)$$

which for nonzero ρ eventually becomes very large, thus relatively shortening the remaining bundle lifetime compared to $\rho=0$.

These results motivate further interpretation in terms of a comparison with what might be expected for ELS bundles under the same fiber parameters. To this end, we consider results in Phoenix [28] in the case of large ELS bundles, since ELS and LLS bundles were found in Newman and Phoenix [6] to have very similar behavior for $0 < \rho < 1$ and $\beta=1$. One asymptotic result in Phoenix [28] for the mean was

$$\begin{aligned} t_N &\approx t_{\text{ref}} \left(\frac{L}{\ell_{\text{ref}}} \right)^{-\rho} \int_0^\infty \exp(-\rho z^\beta) dz \\ &= t_{\text{ref}} \left(\frac{L}{\ell_{\text{ref}}} \right)^{-\rho} \rho^{-1/\beta} \Gamma\left(1 + \frac{1}{\beta}\right). \end{aligned} \quad (23)$$

This result shows that the lifetime, though large, is eventually bounded as $N \rightarrow \infty$ despite the impression given by Fig. 5 for the case $\beta=0.2$ and $\rho=0.1$ and additional calculations mentioned for $\beta=0.1$. In fact, for $L=\ell_{\text{ref}}$, the limiting value will be of order $5! \times 10^5 \approx 1.2 \times 10^7$, which is certainly consistent with the behavior seen in Fig. 5. For the standard

deviation, Phoenix [28] also gives the asymptotic result

$$\sigma_N \approx t_{\text{ref}} \frac{\rho}{\sqrt{N}} \left(\frac{L}{\ell_{\text{ref}}} \right)^{-\rho} \times \left\{ \int_0^\infty \int_0^\infty \mathcal{F}(z_1, z_2) dz_1 dz_2 \right\}^{1/2}, \quad (24)$$

where

$$\mathcal{F}(z_1, z_2) = \exp[-(\rho-1)(z_1^\beta + z_2^\beta)] \Gamma(z_1, z_2), \quad (25)$$

and

$$\Gamma(z_1, z_2) = \{1 - \exp[-\min(z_1^\beta, z_2^\beta)]\} \times \exp[-\max(z_1^\beta, z_2^\beta)], \quad (26)$$

which can be expressed as

$$\sigma_N \approx t_{\text{ref}} \sqrt{\frac{2}{N}} \left(\frac{L}{\ell_{\text{ref}}} \right)^{-\rho} \rho \sqrt{K(\rho-1, \rho; \beta) - K(\rho, \rho; \beta)}, \quad (27)$$

where

$$K(\rho', \rho; \beta) = \int_0^\infty \int_0^{z_2} \exp(-\rho' z_1^\beta) \exp(-\rho z_2^\beta) dz_1 dz_2. \quad (28)$$

It can be shown that

$$K(\rho, \rho; \beta) = \frac{\Gamma^2(1+1/\beta)}{2\rho^{2/\beta}}; \quad (29)$$

however, the integral $K(\rho-1, \rho; \beta)$ fails to converge for $0 < \rho \leq 1/2$. The transitional nature of $\rho=1/2$ was shown in Newman and Phoenix [6] for $\beta=1$, where CV_N decreased as $(N \ln N)^{-1/2}$ and the above results suggest this same transition also occurs for other values of β in the case of ELS.

Figure 16 suggests that $\rho=1/2$ might, perhaps, be a transitional value under LLS as well, but only for large β . Such differences between LLS and ELS might be anticipated for $\rho=1/2$ (or other values less than unity) since for a given configuration of failed and surviving fibers at time t , which from the load sharing law determines the surviving fiber loads, the sum of these loads individually raised to the power ρ will be smaller under LLS than ELS, thus suggesting a smaller fiber failure rate in the former and perhaps a longer and more variable lifetime. Unfortunately, proving such conjectures for $\beta \neq 1$ appears to be difficult. Overall, these results underscore the difficulty in attempting to determine the behavior of the lifetime distribution for bundles of small ρ and β since $N=10^6$ fibers is too small to determine the ultimate limiting behavior.

IV. BRITTLE-LIKE BEHAVIOR FOR $\rho > 1$

A. Monte Carlo results

Next, we consider the cases where $\rho > 1$. Figure 17 shows simulation results for $G_N(t)$ for $\rho=4$ and $\beta=0.1$ plotted on Weibull coordinates whereby $\ln\{-\ln[1-G_N(t)]\}$ vs. $\ln t$ would plot as a straight line if $G_N(t)$ were truly a Weibull distribu-

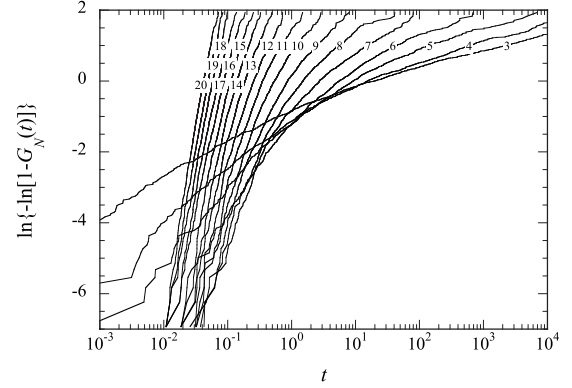


FIG. 17. Lifetime distributions $G_N(t)$ for $\rho=4$ and $\beta=0.1$, with $N=2^m$, $m=3, 4, 5, \dots, 20$ plotted on Weibull probability coordinates.

tion. We see that the bundle lifetime progressively decreases with increasing size but the relative variability dramatically decreases as well. Furthermore, the behavior becomes more Weibull-like for the largest bundles (which would be especially apparent if the horizontal scale were stretched).

As in Newman and Phoenix [6], we consider the reverse weakest-link scaling

$$W_N(t) = 1 - [1 - G_N(t)]^{1/N}, \quad (30)$$

or

$$\ln\{-\ln[1 - W_N(t)]\} = \ln\{-\ln[1 - G_N(t)]\} - \ln N, \quad (31)$$

appropriate to Weibull coordinates.

Figure 18 shows data for $\rho=4$ and $\beta=0.2$ but this time rescaled by this transformation, Eqs. (30) and (31). The lifetime range for all bundle sizes, even when rescaled, spans about five orders of magnitude. As $N \rightarrow \infty$, however, the convergence to one limiting distribution function shape, which we will call $W(t)$, is extremely rapid and by $N=256$ the convergence is essentially complete over the full 1024 point simulation range. Note, however, that for higher values of $\ln\{-\ln[1 - W_N(t)]\}$, the convergence is complete for even smaller N and the reverse would have been observable for

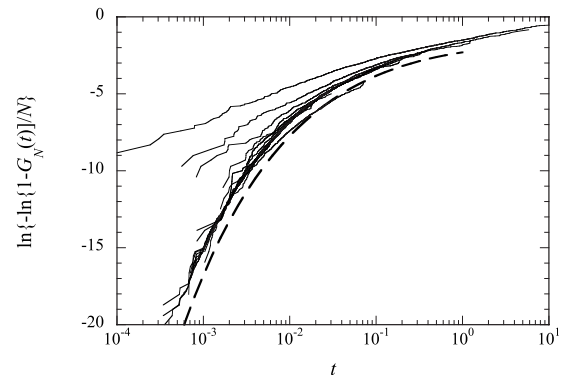


FIG. 18. Convergence of cumulative lifetime distribution functions $W_N(t) = 1 - [1 - G_N(t)]^{1/N}$, plotted using Weibull probability coordinates for $\rho=4$, and $\beta=0.2$ with $N=2^m$, for $m=3, 4, 5, \dots, 20$. The theoretical dashed line is calculated using Eq. (53).

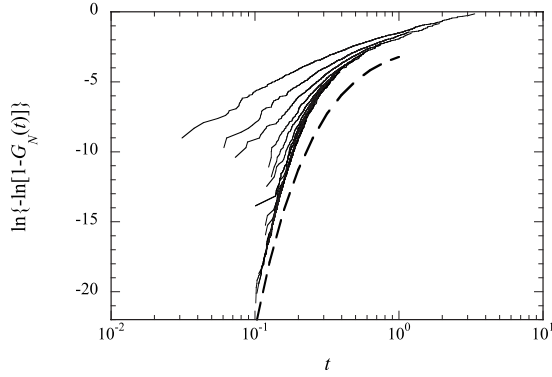


FIG. 19. Convergence of cumulative lifetime distribution functions $W_N(t) = 1 - [1 - G_N(t)]^{1/N}$, plotted using Weibull probability coordinates for $\rho=2$, and $\beta=0.5$ with $N=2^m$, for $m=3, 4, 5, \dots, 20$. The theoretical dashed line is calculated using Eq. (53).

lower values had the replication size been much larger than 1024 points. This convergence indicates that we know the limiting behavior of $W_N(t)$ down to a probability of level of at least $e^{-19} \approx 10^{-8}$.

Very similar behavior is seen for several other cases as shown in Figs. 19–22. Looking also at the figures in Newman and Phoenix [6], we can conclude that the higher the values of either β or ρ , the more rapid the convergence in bundle size N and, in fact, the convergence rate seems to be governed by the product $\beta\rho$. On the other hand, the range spanned by time t in orders of magnitude is strongly driven by the magnitude of ρ but increasing β tends to reduce this range.

B. Theoretical model

To understand this behavior, we consider the fixed load $\ell(t) = L > 0$ on the bundle although we retain $t_{\text{ref}} = \ell_{\text{ref}} = 1$. This leads to a time constant $t_L = L^{-\rho}$ in the problem. Generally, the time constant is $t_L = t_{\text{ref}}(L/\ell_{\text{ref}})^{-\rho}$. To calculate the distribution function $G_N^{(k)}(t)$ for the time to formation of a cluster of contiguous breaks of length k , we appeal to results

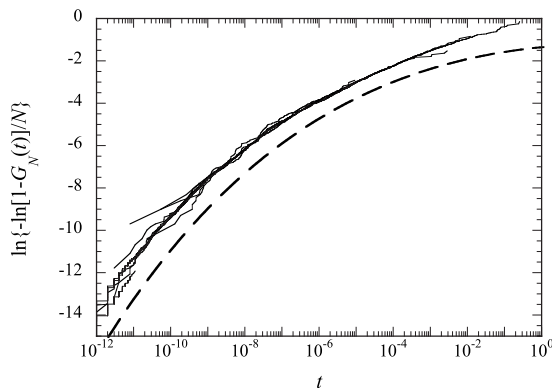


FIG. 20. Convergence of cumulative lifetime distribution functions $W_N(t) = 1 - [1 - G_N(t)]^{1/N}$, plotted using Weibull probability coordinates for $\rho=20$, and $\beta=0.2$ with $N=2^m$, for $m=3, 4, 5, \dots, 20$. The theoretical dashed line is calculated using Eq. (53).

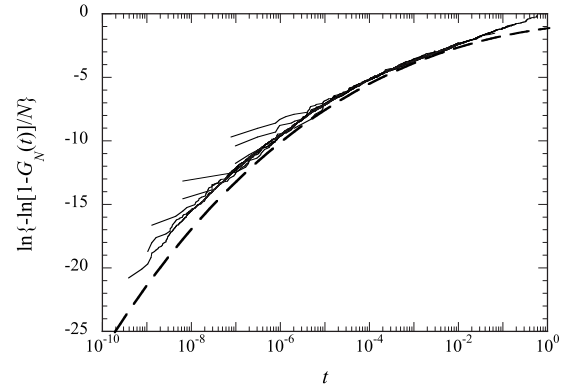


FIG. 21. Convergence of cumulative lifetime distribution functions $W_N(t) = 1 - [1 - G_N(t)]^{1/N}$, plotted using Weibull probability coordinates for $\rho=20$, and $\beta=0.5$ with $N=2^m$, for $m=3, 4, 5, \dots, 20$. The theoretical dashed line is calculated using Eq. (53).

in Phoenix and Tierney [11] where it is shown for large N and $t \ll t_{\text{ref}}$ that

$$G_N^{(k)}(t) \approx 1 - \exp[-Nc_k(L)t^{k\beta}], \quad t \geq 0, \quad (32)$$

where

$$c_k(L) = L^{k\rho\beta} \frac{\Gamma(\beta+1)^k}{\Gamma(k\beta+1)} 2^{k-1} \prod_{j=1}^k K_{j-1}^{\rho\beta}. \quad (33)$$

Motivated by the behavior seen in Figs. 18–22, we wish to approximate the lifetime distribution function $G_N(t)$ by the continuous form

$$G_N(t) = 1 - \exp[-NW(t)], \quad (34)$$

where $W(t)$ is called the characteristic distribution function for lifetime. To this end, we consider the intersections of $G_N^{(k)}(t)$ and $G_N^{(k+1)}(t)$, which ought to occur very close to the limiting curves seen in Figs. 18–22. This yields the intersection points t_k given by

$$c_k(L)t_k^{k\beta} = c_{k+1}(L)t_k^{(k+1)\beta}, \quad k \geq 1, \quad (35)$$

which reduces to

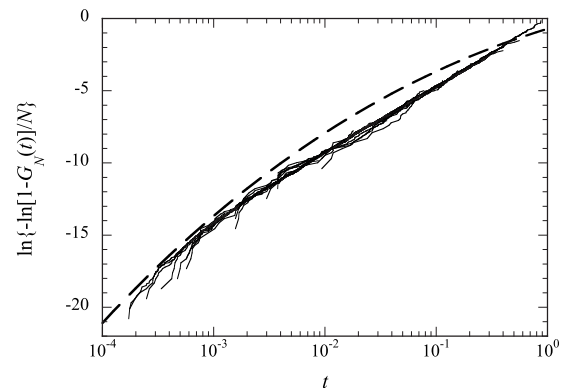


FIG. 22. Convergence of cumulative lifetime distribution functions $W_N(t) = 1 - [1 - G_N(t)]^{1/N}$, plotted using Weibull probability coordinates for $\rho=20$, and $\beta=2.0$ with $N=2^m$, for $m=3, 4, 5, \dots, 20$. The theoretical dashed line is calculated using Eq. (53).

$$t_k^\beta = L^{-\rho\beta} \frac{\Gamma[(k+1)\beta+1]}{2\Gamma(\beta+1)\Gamma(k\beta+1)} \left(\frac{2}{k+2}\right)^{\rho\beta}, \quad (36)$$

or

$$t_k = L^{-\rho} \left\{ \frac{\Gamma[(k+1)\beta+1]}{2\Gamma(\beta+1)\Gamma(k\beta+1)} \right\}^{1/\beta} \left(\frac{2}{k+2}\right)^\rho. \quad (37)$$

We then consider W_k^* defined as

$$\begin{aligned} W_k^* &= c_k(L) t_k^{k\beta} \\ &= L^{k\rho\beta} \frac{\Gamma(\beta+1)^k}{\Gamma(k\beta+1)} 2^{k-1} \prod_{j=1}^k \left(\frac{j+1}{2}\right)^{\rho\beta} \\ &\quad \times L^{-k\rho\beta} \frac{\Gamma[(k+1)\beta+1]^k}{[2\Gamma(\beta+1)\Gamma(k\beta+1)]^k} \left(\frac{2}{k+2}\right)^{k\rho\beta} \\ &= \frac{\Gamma[(k+2)\beta+1-\beta]^k}{2\Gamma[(k+2)\beta+1-2\beta]^{k+1}} \left[\frac{(k+2)!}{(k+2)^{k+2}} \right]^{\rho\beta} \times (k+2)^{\rho\beta}. \end{aligned} \quad (38)$$

Since

$$\Gamma(az+b) \approx \sqrt{2\pi} \exp(-az) (az)^{az+b-1/2}, \quad (39)$$

and $(k+2)! = \Gamma(k+3)$, we can approximate W_k^* as

$$\begin{aligned} W_k^* &\approx \frac{(k+2)^{\rho\beta}}{2} (2\pi)^{\rho\beta/2} (k+2)^{\rho\beta/2} \exp[-(k+2)\rho\beta] \\ &\quad \times (2\pi)^{k/2} [(k+2)\beta]^{k[(k+2)\beta+1-\beta]-k/2} \times \exp[-k(k+2)\beta] \\ &\quad \times (2\pi)^{-(k+1)/2} \times [(k+2)\beta]^{-(k+1)[(k+2)\beta+1-2\beta]+(k+1)/2} \\ &\quad \times \exp[(k+1)(k+2)\beta], \end{aligned} \quad (40)$$

which simplifies to

$$W_k^* \approx \frac{(\sqrt{2\pi})^{\beta\rho-1}}{2\sqrt{\beta}} (k+2)^{(3\beta\rho-1)/2} \exp[-\beta(\rho-1)(k+2)]. \quad (41)$$

Next we obtain a relationship between t_k and $k+2$ and noting first that

$$\begin{aligned} \frac{\Gamma[(k+1)\beta+1]}{\Gamma(\beta+1)\Gamma(k\beta+1)} &= \frac{\Gamma[(k+2)\beta+1-\beta]}{\Gamma(\beta+1)\Gamma[(k+2)\beta+1-2\beta]} \\ &= \frac{[\beta(k+2)]^\beta}{\Gamma(\beta+1)}, \end{aligned} \quad (42)$$

we see that

$$t_k = L^{-\rho} \frac{\beta(k+2)}{[2\Gamma(\beta+1)]^{1/\beta}} \left(\frac{2}{k+2}\right)^\rho. \quad (43)$$

Dropping the subscript k on t to allow it to be a continuous variable, we can invert the above expressions to yield

$$k+2 \approx (L^\rho t)^{-1/(\rho-1)} \left[\frac{\beta 2^{\rho-1/\beta}}{\Gamma(\beta+1)^{1/\beta}} \right]^{1/(\rho-1)}. \quad (44)$$

Finally, we let $W(t) = W_{k(t)}^*$ and thus obtain

$$W(t) \approx C \left(\frac{a}{L^\rho t}\right)^{\phi(\rho-1)} \exp\left[-\beta(\rho-1) \left(\frac{a}{L^\rho t}\right)^{1/(\rho-1)}\right], \quad (45)$$

where

$$\phi = \frac{3\beta\rho-1}{2}, \quad (46)$$

$$a = \frac{\beta 2^{\rho-1/\beta}}{\Gamma(\beta+1)^{1/\beta}}, \quad (47)$$

and

$$C = \frac{(\sqrt{2\pi})^{\rho\beta-1}}{2\sqrt{\beta}}. \quad (48)$$

This version of $W(t)$ corresponds to the time it takes to develop a single critical cluster, but does not include the time to grow across the bundle. We note that the form of the constant $C = C(\rho, \beta)$ depends on how we use the approximation for the Gamma function given above where we expanded in terms of $\beta(k+2)$ to match the $(k+2)/2$ coming from the load sharing. Note, however, when $\beta=1$ that we directly have through Stirling's approximation that

$$\frac{\Gamma[(k+1)\beta+1]^k}{2\Gamma[k\beta+1]^{k+1}} = \frac{(k+1)^{k+1}}{(k+1)!} = \frac{\exp(k+1)}{\sqrt{k+1}}, \quad (49)$$

which leads to an additional factor of $\exp(-1/2)$ in $C(\rho, 1)$. Had we previously expanded this quantity in terms of $\beta(k+1)$, we would obtain the additional factor $\exp[(1-2\beta)/2]$ in $C(\rho, \beta)$ above and for $\beta=1$ this again yields the factor $\exp(-1/2)$ in $C(\rho, 1)$. Thus, we do not know the constant $C(\rho, \beta)$ exactly, but this turns out to be a trivial difference in light of the many orders of magnitude ranges in both time t and probabilities of failure we encounter, as for instance in Figs. 18–22.

Turning to the critical cluster size k^* , we note that it is the value of $k(t)$ that solves $NW_{k(t)}^* = 1$. It can be shown that

$$k^* + 2 = \frac{\log(CN)}{\beta(\rho-1)} (1 + \varepsilon_N), \quad (50)$$

where

$$\varepsilon_N \approx \frac{\phi\{\log \log(CN) - \log[\beta(\rho-1)]\}}{\log(CN) - \phi}. \quad (51)$$

The size effect for the associated critical time t^* for formation of the critical cluster is

$$t^* \approx \frac{a}{L^\rho} \left[\frac{\beta(\rho-1)}{\log(CN)(1 + \varepsilon_N)} \right]^{\rho-1}. \quad (52)$$

Corresponding to the time it takes to form a critical cluster and fail the bundle, a good approximation resulting from matching with the strength version of the problem [29] is

$$W(t) \approx C \left(\frac{a}{L^\rho t} \right)^{\phi(\rho-1)} \exp \left\{ - \left[1 + \frac{\pi^2/6}{\beta^2(\rho-1)^2} \right] \times \beta(\rho-1) \left(\frac{a}{L^\rho t} \right)^{1/(\rho-1)} \right\}, \quad (53)$$

where the additional factor inside the square brackets represents the additional time it takes for the single dominating cluster or “crack” that emerges to traverse the whole specimen. A factor such as this was found also in [6]. However, comparison with the time independent strength problem [29], and noting that the fiber strength Weibull shape parameter is essentially $\approx \beta\rho$ in the current context, leads to the quantity $\beta^2(\rho-1)^2$ in the denominator of the additional factor. (The adjustment from ρ to $\rho-1$ is motivated by the observed critical transition occurring at $\rho=1$.) This form of $W(t)$ obviously tracks the simulations in Figs. 17–21 remarkably well, especially in view of the drastic differences in time scales among these figures. Thus the lifetime distribution for the bundle is given by Eq. (34) with Eq. (53) for the case $\rho > 1$.

Finally, the size effect on time to failure is

$$t_N \approx \frac{a}{L^\rho} \left[\left(1 + \frac{\pi^2/6}{\beta^2(\rho-1)^2} \right) \frac{\beta(\rho-1)}{\log(CN)(1+\varepsilon_N)} \right]^{\rho-1}. \quad (54)$$

V. CONCLUSIONS

We have studied the behavior of a previously introduced, one-dimensional FBM consisting of N fibers under LLS where life consumption in an a fiber followed a power law in its load level, with exponent ρ , and integrated over time. This life consumption function was further embodied in a Weibull functional form resulting in a Weibull distribution for lifetime under constant fiber stress and with exponent (shape parameter), β . We have developed asymptotic results complemented by Monte Carlo simulation using a computational algorithm from our previous work [6] that greatly increases the size, N , of treatable bundles (e.g., 10^6 fibers in 10^3 realizations). Specifically, our algorithm, developed in Newman and Phoenix [6] is $\mathcal{O}(N \ln N)$ in contrast with former algorithms which were $\mathcal{O}(N^2)$.

Regimes were found for various (β, ρ) pairs that yielded drastically contrasting behavior as N increased. For $\rho > 1$ and large N brittle weakest volume behavior emerged expressed in terms of characteristic elements (groupings of fibers) derived from critical cluster formation, and the lifetime eventually but slowly goes to zero in this regime as N approaches ∞ . For $1/2 \leq \rho \leq 1$, however, LLS had remarkably similar behavior to ELS (appearing to have identical lifetime distributions at $\rho=1$) with an asymptotic Gaussian lifetime distribution and a finite limiting mean for large N . The coefficient of variation in lifetime, followed a power law in increasing N , but except for $\rho=1$, the value of the negative exponent was clearly less than $1/2$ (characteristic of the central limit

theorem) unlike in ELS bundles where the exponent remains $1/2$ for $1/2 < \rho \leq 1$.

For sufficiently small values $0 < \rho \leq 1$, a transition occurred, depending on β , whereby LLS bundle lifetimes became dominated by a few long-lived fibers (perhaps acting in a group). Thus the bundle lifetime appeared to approximately follow an extreme-value distribution for the longest lived of a parallel group of statistically independent elements, which applied exactly to the case $\rho=0$. The lower the value of β , the higher the transition value of ρ , below which such extreme value behavior occurred. No evidence was found for limiting Gaussian behavior for values of $\rho > 1$ but with $0 < \beta(\rho+1) < 1$, as one might have conjectured based on the behavior of quasistatic models for bundle strength, where the role of the Weibull exponent for fiber strength is played by $\beta(\rho+1)$.

As a final comment, Weibull lifetime behavior and power-law sensitivity of lifetime to load level are ubiquitous features of structural elements, which themselves may be built up from hierarchical substructures with elongated anisotropic characteristics. For instance, polymer-derived fibers with micron-scale diameters (e.g., aramid, carbon, PBO, UHM-WPE) are constructed of oriented fibrils or crystallites, which themselves are collections of aligned molecules. While the molecular bonds themselves are generally viewed as having exponentially distributed lifetimes, this is not true of the higher level structures in the hierarchy (the fibers) which can have more Weibull-like behavior with β that can be much larger or smaller than unity. Furthermore, whether the higher level structures behave in a brittle or a ductile like fashion depends on many factors, but especially temperature. Phoenix and Tierney [7] have presented molecular level arguments that ρ is inversely proportional to absolute temperature and in the current context that would imply a transition, eventually from brittle-to-ductile like behavior. However the exact transition value of ρ is expected to depend in the dimensionality of the material and the severity of localization of the stress-redistribution mechanism. The current work assumes, perhaps the most severe case in a 1D array, and thus the transition value for ρ is unity, whereas real materials will have much milder, local load sharing with many more neighbors involved. This is likely to increase the ρ value where a brittle-to-ductile transition might occur. The importance of the current work is to show that, apart from the issue of the precise transition value of ρ , the characteristics of the lifetime distributions can be expected to be complex. Much more work is needed to understand the broader range of transition values for ρ , that are possible in real materials for the brittle-to-ductile transition.

ACKNOWLEDGMENTS

S.L.P. acknowledges support from the U.S. National Institute of Justice under DoJ Agreement ID: Grant No. 2007-DE-BX-K003.

- [1] C. Moukarzel and P. M. Duxbury, *J. Appl. Phys.* **76**, 4086 (1994); P. M. Duxbury, P. D. Beale, and C. Moukarzel, *Phys. Rev. B* **51**, 3476 (1995).
- [2] N. M. Pugno, *J. Phys.: Condens. Matter* **18**, S1971 (2006); *Acta Mater.* **55**, 5269 (2007).
- [3] B. Q. Wu and P. L. Leath, *Phys. Rev. B* **61**, 15028 (2000); **62**, 9338 (2000).
- [4] J. Boksiner and P. L. Leath, *Phys. Rev. E* **67**, 066610 (2003).
- [5] P. L. Leath and P. M. Duxbury, *Phys. Rev. B* **49**, 14905 (1994).
- [6] W. I. Newman and S. L. Phoenix, *Phys. Rev. E* **63**, 021507 (2001).
- [7] P. C. Hemmer and A. Hansen, *ASME J. Appl. Mech.* **59**, 909 (1992).
- [8] U. Divakaran and A. Dutta, *Phys. Rev. E* **75**, 011117 (2007).
- [9] R. C. Hidalgo, K. Kovaks, I. Pagonabarraga, and F. Kun, *Europhys. Lett.* **81**, 54005 (2008).
- [10] J. B. Gomez, D. Iniguez, and A. F. Pacheco, *Phys. Rev. Lett.* **71**, 380 (1993).
- [11] S. L. Phoenix and L.-J. Tierney, *Eng. Fract. Mech.* **18**, 193 (1983).
- [12] B. D. Coleman, *Trans. Soc. Rheol.* **1**, 153 (1957); **2**, 195 (1958); *J. Appl. Phys.* **29**, 968 (1958).
- [13] W. A. Curtin and H. Scher, *Phys. Rev. B* **45**, 2620 (1992); **55**, 12038 (1997).
- [14] W. A. Curtin, M. Pamel, and H. Scher, *Phys. Rev. B* **55**, 12051 (1997).
- [15] O. E. Yewande, Y. Moreno, F. Kun, R. C. Hidalgo, and H. J. Herrmann, *Phys. Rev. E* **68**, 026116 (2003); R. C. Hidalgo, Y. Moreno, F. Kun, and H. J. Herrmann, *ibid.* **65**, 046148 (2002).
- [16] A. Guarino, L. Vanel, R. Scorretti, and S. Ciliberto, *J. Stat. Mech.* 2006, P06020; A. Politi, S. Ciliberto, and R. Scorretti, *Phys. Rev. E* **66**, 026107 (2002); R. Scorretti, S. Ciliberto, and A. Guarino, *Europhys. Lett.* **55**, 626 (2001).
- [17] N. Yoshioka, F. Kun, and N. Ito, *Phys. Rev. Lett.* **101**, 145502 (2008).
- [18] R. Toussaint and A. Hansen, *Phys. Rev. E* **73**, 046103 (2006).
- [19] S. Pradhan and A. Hansen, *Phys. Rev. E* **72**, 026111 (2005).
- [20] F. Raischel, F. Kun, and H. J. Herrmann, *Phys. Rev. E* **74**, 035104(R) (2006).
- [21] S. Pradhan, P. Bhattacharyya, and B. K. Chakrabarti, *Phys. Rev. E* **66**, 016116 (2002).
- [22] M. J. Alava, P. K. V. V. Nukala, and S. Zapperi, *Phys. Rev. Lett.* **100**, 055502 (2008); *Int. J. Fract.* **154**, 51 (2008).
- [23] M. J. Alava, P. K. V. V. Nukala, and S. Zapperi, *J. Phys. D* (to be published).
- [24] S. Roux, *Phys. Rev. E* **62**, 6164 (2000).
- [25] S. Roux and F. Hild, *Int. J. Fract.* **116**, 219 (2002).
- [26] Y. Charles, F. Hild and S. Roux, *ASME J. Eng. Mater. Technol.* **125**, 333 (2003).
- [27] Z. P. Bazant and S.-D. Pang, *Proc. Natl. Acad. Sci. U.S.A.* **103**, 9434 (2006); *J. Mech. Phys. Solids* **55**, 91 (2007); S.-D. Pang, Z. P. Bazant, and J. L. Le, *Int. J. Fract.* **154**, 131 (2008).
- [28] S. L. Phoenix, *SIAM (Soc. Ind. Appl. Math.) J. Numer. Anal.* **34**, 227 (1978).
- [29] S. Mahesh, S. L. Phoenix, and I. J. Beyerlein, *Int. J. Fract.* **115**, 41 (2002).